Research Article | Vol. 25, No. 12 | 12 Jun 2017 | OPTICS EXPRESS 13577
Optics EXPRESS

Vertically- resolved phytoplankton carbon and net primary production from a high spectral resolution lidar

JENNIFER A. SCHULIEN,[1,*] MICHAEL J. BEHRENFELD,[1] JOHNATHAN W. HAIR,[2] CHRIS A. HOSTETLER,[2] AND MICHAEL S. TWARDOWSKI[3]

[1]*Department of Botany and Plant Pathology, Oregon State University, Corvallis, OR 97331, USA*
[2]*National Aeronautics and Space Administration, Langley Research Center, Hampton VA 23681, USA*
[3]*Harbor Branch Oceanographic Institute, Florida Atlantic University, 5600 US 1 North, Fort Pierce, FL 34946, USA*
[*]*schuliej@oregonstate.edu*

Abstract: Passive ocean observing sensors are unable to detect subsurface structure in ocean properties, resulting in errors in water column integrated phytoplankton biomass and net primary production (NPP) estimates. Active lidar (light detection and ranging) sensors make quantitative measurements of depth-resolved backscatter (b_{bp}) and diffuse light attenuation (K_d) coefficients in the ocean and can provide critical measurements for biogeochemical models. Sub-surface phytoplankton biomass, light, chlorophyll, and NPP fields were characterized using both *in situ* measurements and coincident airborne high spectral resolution lidar (HSRL-1) measurements collected as part of the SABOR (Ship-Aircraft Bio-Optical Research) field campaign. We found that depth-resolved data are critical for calculating phytoplankton stocks and NPP, with improvements in NPP estimates up to 54%. We observed strong correlations between coincident HSRL-1 and *in situ* IOP measurements of both b_{bp} ($r = 0.94$) and K_d ($r = 0.90$).

OCIS codes: (010.0010) Atmospheric and oceanic optics; (280.0280) Remote sensing and sensors; (010.4450) Oceanic optics.

References and links

1. J. H. Churnside, "Bio-optical model to describe remote sensing signals from a stratified ocean," J. Appl. Remote Sens. **9**(1), 095989 (2015).
2. M. G. Jacox, C. A. Edwards, M. Kahru, D. L. Rudnick, and R. M. Kudela, "The potential for improving remote primary productivity estimates through subsurface chlorophyll and irradiance measurement," Deep Sea Res. Part 2 Top. Stud. Oceanogr. **112**, 107–116 (2015).
3. M. Stramska and D. Stramski, "Effects of a nonuniform vertical profile of chlorophyll concentration on remote-sensing reflectance of the ocean," Appl. Opt. **44**(9), 1735–1747 (2005).
4. T. Platt and S. Sathyendranath, "Oceanic primary production: estimation by remote sensing at local and regional scales," Science **241**(4873), 1613–1620 (1988).
5. F. E. Hoge, C. W. Wright, W. B. Krabill, R. R. Buntzen, G. D. Gilbert, R. N. Swift, J. K. Yungel, and R. E. Berry, "Airborne lidar detection of subsurface oceanic scattering layers," Appl. Opt. **27**(19), 3969–3977 (1988).
6. J. H. Churnside, B. J. McCarty, and X. Lu, "Subsurface ocean signals from an orbiting polarization lidar," Remote Sens. **5**(7), 3457–3475 (2013).
7. J. H. Churnside, "Review of profiling oceanographic lidar," Opt. Eng. **53**(5), 051405 (2014).
8. J. Hair, C. Hostetler, Y. Hu, M. Behrenfeld, C. Butler, D. Harper, R. Hare, T. Berkoff, A. Cook, J. Collins, N. Stockley, M. Twardowski, I. Cetinic, R. Ferrare, and T. Mack, "Combined atmospheric and ocean profiling from an airborne high spectral resolution lidar," in *EPJ Web of Conferences* (EDP Sciences, 2016), pp. 22001.
9. J. W. Hair, C. A. Hostetler, A. L. Cook, D. B. Harper, R. A. Ferrare, T. L. Mack, W. Welch, L. R. Izquierdo, and F. E. Hovis, "Airborne high spectral resolution lidar for profiling aerosol optical properties," Appl. Opt. **47**(36), 6734–6752 (2008).
10. M. J. Behrenfeld, E. Boss, D. A. Siegel, and D. M. Shea, "Carbon-based ocean productivity and phytoplankton physiology from space," Global Biogeochem. Cycles **19**(1), 2299 (2005).
11. T. Westberry, M. J. Behrenfeld, D. A. Siegel, and E. Boss, "Carbon-based primary productivity modeling with vertically resolved photoacclimation," Global Biogeochem. Cycles **22**(2), 3078 (2008).

#287974 https://doi.org/10.1364/OE.25.013577
Journal © 2017 Received 6 Mar 2017; accepted 4 May 2017; published 7 Jun 2017

Optics EXPRESS

12. J. W. Campbell and J. E. O'Reilly, "Role of satellites in estimating primary productivity on the northwest Atlantic continental shelf," Cont. Shelf Res. **8**(2), 179–204 (1988).
13. J. E. O'Reilly and C. Zetlin, "Seasonal, horizontal, and vertical distribution of phytoplankton chlorophyll a in the northeast US continental shelf ecosystem," NOAA Technical Report NMFS 139 (1998).
14. M. S. Twardowski, J. M. Sullivan, P. L. Donaghay, and J. R. V. Zaneveld, "Microscale quantification of the absorption by dissolved and particulate material in coastal waters with an ac-9," J. Atmos. Ocean. Technol. **16**(6), 691–707 (1999).
15. J. R. V. Zaneveld, J. C. Kitchen, and C. C. Moore, "Scattering error correction of reflecting-tube absorption meters," in Ocean Optics XII (International Society for Optics and Photonics, 1994), pp. 44–55.
16. J. M. Sullivan, M. S. Twardowski, P. L. Donaghay, and S. A. Freeman, "Use of optical scattering to discriminate particle types in coastal waters," Appl. Opt. **44**(9), 1667–1680 (2005).
17. J. M. Sullivan, M. S. Twardowski, J. R. V. Zaneveld, and C. C. Moore, "Measuring optical backscattering in water," in *Light Scattering Reviews 7*, (Springer Berlin Heidelberg, 2013), pp. 189–224.
18. H. R. Gordon, O. B. Brown, R. H. Evans, J. W. Brown, R. C. Smith, K. S. Baker, and D. K. Clark, "A semianalytic radiance model of ocean color," J. Geophys. Res. Atmos. **93**(D9), 10909–10924 (1988).
19. J. R. Graff, T. K. Westberry, A. J. Milligan, M. B. Brown, G. Dall'Olmo, V. van Dongen-Vogels, K. M. Reifel, and M. J. Behrenfeld, "Analytical phytoplankton carbon measurements spanning diverse ecosystems," Deep Sea Res. Part 1 Oceanogr. Res. Pap. **102**, 16–25 (2015).
20. R. W. Austin and T. J. Petzold, "Spectral dependence of the diffuse attenuation coefficient of light in ocean waters: a reexamination using new data," in *Orlando'90* (International Society for Optics and Photonics, 1990), pp. 79–93.
21. A. Morel, B. Gentili, H. Claustre, M. Babin, A. Bricaud, J. Ras, and F. Tieche, "Optical properties of the "clearest" natural waters," Limnol. Oceanogr. **52**(1), 217–229 (2007).
22. C. de Boyer Montégut, G. Madec, A. S. Fischer, A. Lazar, and D. Iudicone, "Mixed layer depth over the global ocean: an examination of profile data and a profile-based climatology," J. Geophys. Res. Oceans **109**, C12003 (2004).
23. R. M. Letelier, D. M. Karl, M. R. Abbott, and R. R. Bidigare, "Light driven seasonal patterns of chlorophyll and nitrate in the lower euphotic zone of the North Pacific Subtropical Gyre," Limnol. Oceanogr. **49**(2), 508–519 (2004).
24. M. E. Conkright, R. A. Locarnini, H. E. Garcia, T. D. O'Brien, T. P. Boyer, C. Stephens, and J. I. Antonov, World Ocean Atlas 2001: Objective analyses, data statistics, and figures: CD-ROM documentation. US Department of Commerce, National Oceanic and Atmospheric Administration, National Oceanographic Data Center, Ocean Climate Laboratory, (2002).
25. J. R. Zaneveld, A. Barnard, and E. Boss, "Theoretical derivation of the depth average of remotely sensed optical parameters," Opt. Express **13**(22), 9052–9061 (2005).
26. W. J. Moses, S. G. Ackleson, J. W. Hair, C. A. Hostetler, and W. D. Miller, "Spatial scales of optical variability in the coastal ocean: implications for remote sensing and in situ sampling," J. Geophys. Res. Oceans **121**(6), 4194–4208 (2016).
27. P. J. Werdell and S. W. Bailey, "An improved in-situ bio-optical data set for ocean color algorithm development and satellite data product validation," Remote Sens. Environ. **98**(1), 122–140 (2005).
28. M. J. Behrenfeld, Y. Hu, C. A. Hostetler, G. Dall'Olmo, S. D. Rodier, J. W. Hair, and C. R. Trepte, "Space-based lidar measurements of global ocean carbon stocks," Geophys. Res. Lett. **40**(16), 4355–4360 (2013).
29. M. Behrenfeld, Y. Hu, R. O'Malley, E. Boss, C. Hostetler, D. Siegel, J. Sarmiento, J. Schulien, J. Hair, X. Lu, S. Rodier, and A. J. Scarino, "Decade of polar phytoplankton biomass cycles characterized using space-based lidar," Nat. Geosci. (posted 19 December 2016, in press).

1. Introduction

It has been widely recognized since the Coastal Zone Color Scanner (CZCS) era that the inability of passive ocean color measurements to resolve phytoplankton vertical structure can be a primary source of error in global phytoplankton biomass and net primary production (NPP) estimates [1,2]. Stramska and Stramski (2005) [3] used HydroLight to model the effects of non-uniform chlorophyll distributions on remote-sensing reflectance (R_{RS}) and found sub-surface chlorophyll maxima could result in relative errors in chlorophyll (calculated as an R_{RS} ratio) of up to 70% under oligotrophic conditions. Platt and Sathyendranath (1988) [4] evaluated the impact of vertical structure in chlorophyll on integrated NPP measurements and found that errors in NPP were considerably larger when the chlorophyll feature was located in the upper water column. Here we use data collected during the 2104 NASA SABOR (Ship-Aircraft Bio-Optical Research) campaign to evaluate the utility of lidar (light detection and ranging) measurements for characterizing vertical variability in plankton and optical properties. Active lidar sensors make quantitative measurements of depth-resolved backscatter (b_{bp}) and diffuse light attenuation (K_d)

Optics EXPRESS

coefficients in the ocean [5–9] and can provide critical measurements for biogeochemical models.

The SABOR campaign was conducted in the western North Atlantic with the goal of advancing key technologies for plankton characterizations from space. We evaluated sub-surface phytoplankton biomass, light, and chlorophyll fields using both high spectral resolution lidar (HSRL-1) and coincident in-water IOP (inherent optical property) measurements. These data were then employed as inputs to the carbon-based production model (CbPM) [10,11] to calculate vertically resolved NPP. SABOR sampling stations covered continental shelf, slope, and offshore waters and provided a large dynamic range in bio-optical states. Previous work has found that NPP in this region is seasonally variable and often exhibits strong water column stratification and subsurface chlorophyll and production features that persist through the summer season [12,13].

We show that depth-resolved measurements of ocean properties are critical for calculating biomass and NPP in the upper ocean and enable up to 54% more accurate estimates of NPP compared to calculations made without information on the vertical structure. We also show that phytoplankton biomass features of a given magnitude have a significantly larger impact on NPP estimates if they are located in the top two optical depths of the water column compared to deeper features. This critical upper layer can be effectively characterized by either an airborne or satellite ocean-optimized lidar.

2. Methods

The SABOR campaign was conducted onboard the *R/V Endeavor* in the northwest Atlantic from 18 July to 6 August 2014. Profiles of optical properties, conductivity, temperature, and depth (CTD) were collected at 23 stations. Data collected at these stations were used to quantify the effects of vertical structure in phytoplankton biomass, light attenuation, and chlorophyll on NPP calculations. Casts where the photic zone depth was greater than the depth of the water column (5 stations) were excluded from the analyses. Concurrent measurements with an ocean-optimized airborne lidar were compared to in-water measurements and used to evaluate how future satellite lidar data may complement passive ocean color observations to reduce uncertainties in retrieved ocean ecosystem properties.

Ship-based (hereafter referred to as *'in situ')* absorption and attenuation data at 9 wavelengths (412, 440, 488, 510, 532, 555, 650, 676, and 715 nm) were collected using a WET Labs (Philomath, OR) ac-9. The ac-9 was calibrated with Milli-Q ultrapure water following the protocols in Twardowski et al. (1999) [14]. Absorption was corrected for scattering effects using the proportional method of Zaneveld et al. (1994) [15]. Data were corrected for temperature and salinity effects using the coefficients of Twardowski et al. (1999) [14] and *in situ* CTD data (SeaBird SBE49 CTD; Bellevue, WA). Chlorophyll was calculated from phytoplankton absorption using the method of Sullivan et al. (2005) [16]. Backscatter was measured using a WET Labs ECO-BB9 (412, 440, 488, 510, 532, 595, 660, 676, and 715 nm). Backscatter data were linearly interpolated for wavelengths not matching the ac-9 (555 and 650 nm). Volume scattering function data were converted to backscattering coefficients following the protocol in Sullivan et al. (2013) [17]. Light attenuation coefficients at 532 nm were calculated as a function of total absorption at 532 nm, backscattering at 532 nm, and sun angle according to Gordon et al. (1988) [18]. Solar zenith angle was assumed to be 0° for comparison to HSRL-1 measurements. All data were averaged into 1 m depth bins and smoothed using a five-point moving average.

Optics EXPRESS

Table 1. Distances between the HSRL-1 nearest profile and optics cast

STATION	Δ*SPACE (degrees)*	Δ*SPACE (km)**	Δ*TIME (hours)*	Δ*ABS. DISTANCE***
1	0.001	0.093	0.139	0.510
2	0.275	22.825	14.621	57.371
3	0.079	7.058	0.041	7.059
4	0.009	1.022	7.195	25.923
5	0.002	0.173	0.463	1.676
6	0.001	0.117	2.998	10.792
7	0.003	0.244	2.926	10.535
8	0.004	0.367	1.522	5.490
9	0.002	0.167	1.356	4.884
10	7.840E-4	0.083	9.466	34.076
11	0.615	55.071	4.186	57.095
12	0.009	9.026	6.636	25.538
13	0.096	8.492	19.166	69.520
14	0.005	0.370	8.482	30.536
15	0.025	2.044	10.207	36.803
16	0.007	0.580	10.982	39.541
17	0.008	0.787	11.950	43.026
18	1.337	133.207	5.508	134.675

*The spatial differences in degrees were converted to kilometers at latitude using the Haversine function.

**Absolute distance calculated as a function of spatial and temporal differences assuming a current speed of 1 m s^{-1}.

HSRL-1 measurements of ocean b_{bp} and K_d at 532 nm were collected onboard the NASA LaRC King Air aircraft at approximately 9 km altitude [8]. *In situ* optics casts were matched to HSRL-1 measurements within one day and half a degree. On average, HSRL-1 and *in situ* comparisons were made between measurements collected 3.3 km and 6.8 hours apart (Table 1). The median of the ten nearest lidar profiles (~4 km radius) was used for comparisons with *in situ* data. Phytoplankton carbon (C_{phyto}; mg m^{-3}) was calculated from b_{bp} according to Graff et al. (2015) [19] for both *in situ* and HSRL-1 measurements. HSRL-1 C_{phyto} data were converted to chlorophyll concentrations using depth-dependent changes in chlorophyll:C_{phyto} resulting from nutrient-replete photoacclimation [11]:

$$Photoacc\lim ation = 0.022 + (0.045 - 0.022)e^{-3I_g}, \quad (1a)$$

$$Chlorophyll = photoacc\lim ation * C_{phyto}, \quad (1b)$$

where I_g = growth irradiance (see below). Data were smoothed vertically using a five-point moving average. The HSRL-1 data were matched by depth to the *in situ* measurements using linear interpolation, reducing the vertical resolution from 0.94 to 1 m. The HSRL-1 measures ocean properties to approximately 2.5-3 optical depths below the surface. The measured b_{bp} and K_d values below this depth were fixed to the value measured at the maximum penetration depth.

NPP (mg m^{-3} d^{-1}) was calculated using the CbPM where inputs include b_{bp} (m^{-1}), K_d (PAR; m^{-1}), PAR (Ein m^{-2} d^{-1}), mixed layer depth (*MLD*), euphotic zone depth (Z_{eu}), day length (*dl*), nutricline depth, and I_g (Ein m^{-2}). The light attenuation coefficient for PAR was calculated from $K_d(532)$ following Austin and Petzold (1990) [20] and Morel et al. (2007) [21]. PAR was measured using an Eppley PSP (Eppley Laboratories, Newport, RI) mounted to the top of the crane cab eight meters above the waterline. *MLD* was calculated using a fixed density threshold of 0.03 kg m^{-3} following de Boyer Montegut et al. (2004) [22]. The

Optics EXPRESS

CbPM was used to model NPP because calculations are vertically resolved and thus provide depth-dependent values for comparison to calculations with vertically-resolved measurements. Growth irradiance (I_g) is the light level to which phytoplankton are acclimated. Growth irradiance in the mixed layer was calculated as [10,11]:

$$I_g = (PAR * 0.975 / dl) e^{-K_d * \frac{MLD}{2}}, \quad (2)$$

where K_d is the median light attenuation coefficient for PAR in the mixed layer and 0.975 accounts for Fresnel reflection. Growth irradiance at depths below the mixed layer was taken as PAR at that depth. For HSRL-based calculations of chlorophyll, K_d was proportionally adjusted to match the *in situ* data before solving for I_g. Euphotic zone depth was defined as the 0.415 mol quanta m^{-2} d^{-1} isolume depth [23]. Nutrients were not measured as part of SABOR and, thus, nutricline depths employed in the CbPM were taken from the World Ocean Atlas [24]. Stratification indices were calculated by taking the difference between densities at 10 m and 40 m. If the maximum depth was less than 40 m, the density at the maximum depth was used to calculate the stratification index.

A single surface-weighted value was calculated from the *in situ* profiles of K_d and C_{phyto} following Zaneveld et al. (2005) [25]. These values were then extended through the water column to create the unstructured condition used to quantify the effect of uncharacterized vertical structure. Surface measurements of C_{phyto}, the underwater light field, and chlorophyll were used to calculate NPP using the traditional CbPM and compared to NPP calculated with vertically-resolved measurements. Percent relative error (δ_{rel}) was used as a measure of vertical structure and calculated as:

$$\partial_{rel}(\%) = 100 * \frac{\partial_{rel}}{\bar{y}}, \quad (3a)$$

$$\partial_{rel} = \frac{\sum_{i=1}^{n} (y_i - \hat{y}_i)}{n}, \quad (3b)$$

where y_i and $\hat{y}_j$ are the measured ocean properties from, respectively, a uniform and vertically-resolved water column at depth i, and $\bar{y}$ is equal to the mean of the vertically-resolved measurements. This metric gives no indication of the residual magnitudes, so the percent mean absolute error (δ) was also calculated:

$$\partial(\%) = 100 * \frac{\partial}{\bar{y}}, \quad (4a)$$

$$\partial = \frac{\sum_{i=1}^{n} | y_i - \hat{y}_i |}{n}. \quad (4b)$$

These metrics were also used to compare the HSRL-1 to *in situ* measurements where y_i and $\hat{y}_i$ are the *in situ* and HSRL-1 measurements of ocean properties, respectively, and $\bar{y}$ is the mean of the *in situ* values. Pearson correlation coefficients were used to compare HSRL-1 and *in situ* measurements and additionally to evaluate depth-dependent differences between measurements. Finally, percent root mean square error (%RMSE) was calculated as:

Optics EXPRESS

$$RMSE(\%) = 100 * \frac{RMSE}{\bar{y}}, \tag{5a}$$

$$RMSE = \sqrt{\frac{\sum_{i=1}^{n} (y_i - \square_i)^2}{n}}. \tag{5b}$$

3. Results

3.1 In situ data

Phytoplankton and optical properties exhibited significant vertical structure at each SABOR station. Comparison of euphotic zone-integrated C_{phyto} values (ΣC_{phyto}) calculated using depth-resolved *in situ* data and values based solely on surface properties within the passive ocean color detection layer produced δ_{rel} values ranging from –45.6% to –6.2% ($\bar{\delta}_{rel}$ = –19.9%) (Fig. 1(a)). The 'ocean color type' values thus consistently underestimated ΣC_{phyto} at all stations. Furthermore, previous studies in the region have shown that sub-surface chlorophyll structure is observed under stratified conditions [13]. In a similar manner, we found that the largest relative errors were correlated with the stratification index (r = 0.72). Comparison of depth-resolved and surface-only based $K_d(532)$ values showed a similar degree of discrepancy, with δ_{rel} values ranging from –36.3% to –2.7% ($\bar{\delta}_{rel}$ = –20.2%) (Fig. 1(b)). Largest relative errors in depth-integrated K_d (ΣK_d) were correlated, though not as strongly, with the stratification index (r = 0.52).

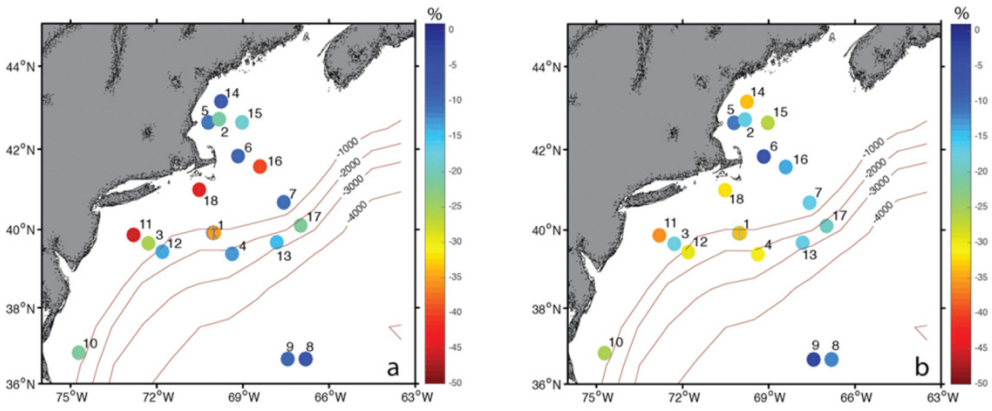

Fig. 1. SABOR stations plotted as a function of percent relative error in (a) C_{phyto} and (b) $K_d(532)$, where percent relative error is a measure of vertical structure. Isobaths are plotted at 1000 m intervals.

Knowledge of the vertical variability in C_{phyto} and K_d is critical to obtaining accurate column and vertically-resolved estimates of NPP. We tested the significance of this structure by comparing vertically-resolved calculations of NPP to values where uniform properties were assumed from surface-weighted properties, as would be applied to passive ocean color data. The vertically-resolved *in situ* C_{phyto} and K_d data enabled much more accurate estimates of NPP compared to calculations made without information on the vertical structure (δ_{rel} = –43.2 – 54.0%; $\bar{\delta}_{rel}$ = –8.4% and δ = 11.7 – 54.0%; $\bar{\delta}$ = 33.4%) (Fig. 2). Larger absolute errors, or differences between *in situ* measurements and an assumed constant profile, were observed deeper in the water column, leading to larger absolute differences in sub-surface NPP. To understand the relative impact of C_{phyto} on NPP calculations as a function of depth, errors in NPP were normalized to C_{phyto} errors and binned by optical depth. Normalized NPP

Optics EXPRESS

errors decreased exponentially from the first to third optical depths. Thus, biomass features located near the surface had a significantly larger impact on NPP estimates than errors located deeper in the water column.

HSRL-1 retrieves optical properties that are limited to the first 2.5-3 optical depths. Therefore, *in situ* values of b_{bp} and K_d from three optical depths to the bottom of the photic zone were held constant to test how much error is introduced to integrated biomass and light attenuation calculations when this modification is applied. Mean absolute errors were only 4.4% and 3.1% for C_{phyto} and K_d, respectively, indicating that applying this extrapolation to HSRL-1 data at depth has only a small effect on integrated biomass and light calculations in the photic zone.

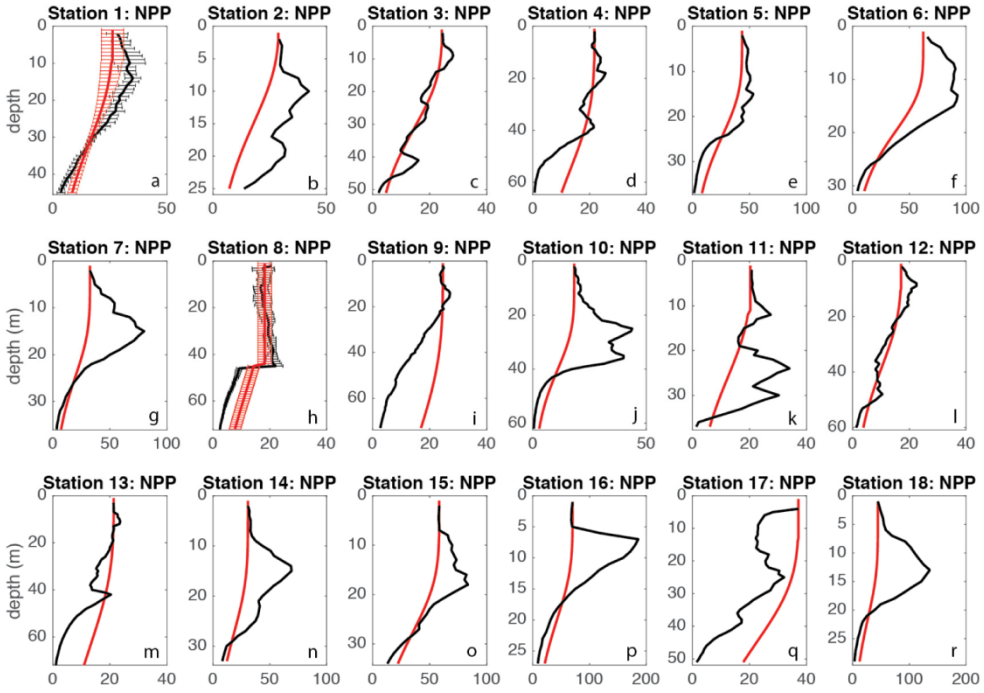

Fig. 2. NPP (mg C m^{-3} d^{-1}) profiles from the carbon-based production model (CbPM) at every station where the maximum depth is greater than the euphotic depth. The black lines are the *in situ* optics-based estimates. The profiles which use surface-weighted values in the traditional CbPM are shown in blue. Panels (a) and (h) are the stations with replicate casts ($\Delta t < 1$ day, same station) with the error bars representing one standard deviation.

3.2 HSRL-1 measurements of ocean properties

A strong correlation ($r = 0.94$) was observed between *in situ* and HSRL-1 measurements of b_{bp} (Fig. 3(a)). Similarly, *in situ* and HSRL-1 values of K_d also showed high correlation ($r = 0.90$) (Fig. 3(b)). The HSRL-1 measurements of b_{bp} and K_d were high compared to *in situ* data, with δ_{rel} values of −9.26% and −12.92% for b_{bp} and K_d, respectively. Measurement differences were not correlated with depth for b_{bp} or K_d ($r = 0.18$ and −0.13).

Optics EXPRESS

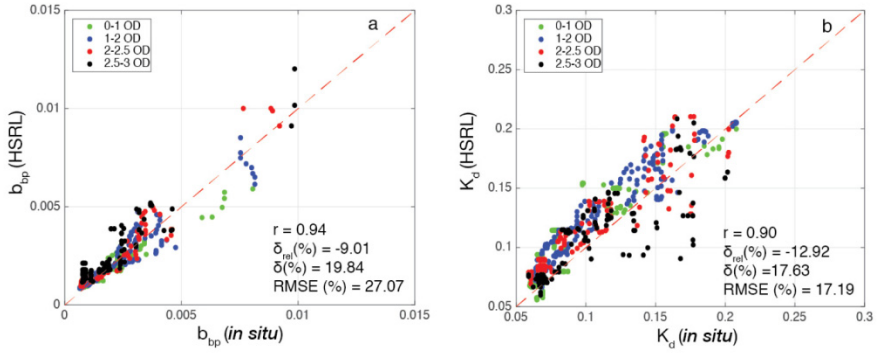

Fig. 3. HSRL-1 and *in situ* measurements of (a) b_{bp} (m^{-1}) and (b) K_d (m^{-1}) with marker color indicating optical depth. The dotted red lines show the 1:1 relationship.

Spatial and temporal variability in geophysical properties is one factor contributing to differences between *in situ* and HSRL-1 retrievals and this issue may be particularly important in the highly variable region studied during SABOR. HSRL-1 and *in situ* profiles were often collected more than 10 km away. Given the spatial scale of variability in coastal waters (~200 m) observed by Moses et al. (2016) [26], we would expect differences between the two measurements (Figs. 4 and 5). When we applied more stringent matchup criteria (<0.01° and <3 hours) [27], only 7 profiles were available for comparison. Surprisingly, the correlation coefficients for b_{bp} decreased slightly to 0.92 and increased to 0.92 for K_d.

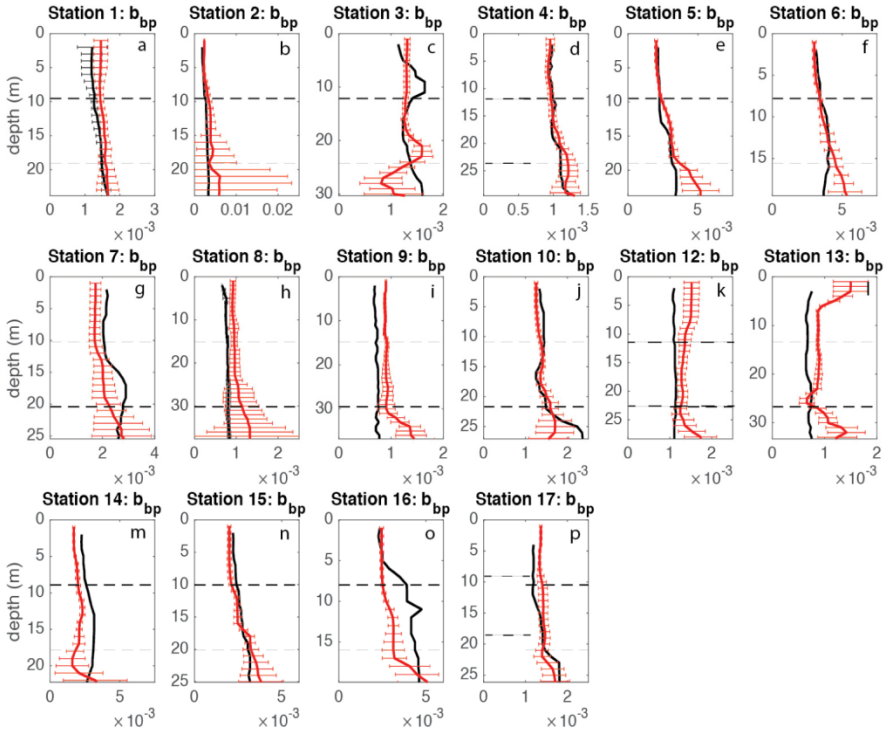

Fig. 4. HSRL-1 and *in situ* measurements of b_{bp} (m^{-1}). The black profiles are the *in situ* measurements where panels (a) and (h) show the stations with replicate casts ($\Delta t < 1$ day, same station) with the error bars representing one standard deviation. The red profiles are the HSRL-1 measurements (median of ten nearest profiles to *in situ* cast) with the error bars representing one standard deviation within profiles. The error bars are a measure of the spatial variability around each station. The dotted lines show the first and second optical depths.

Optics EXPRESS

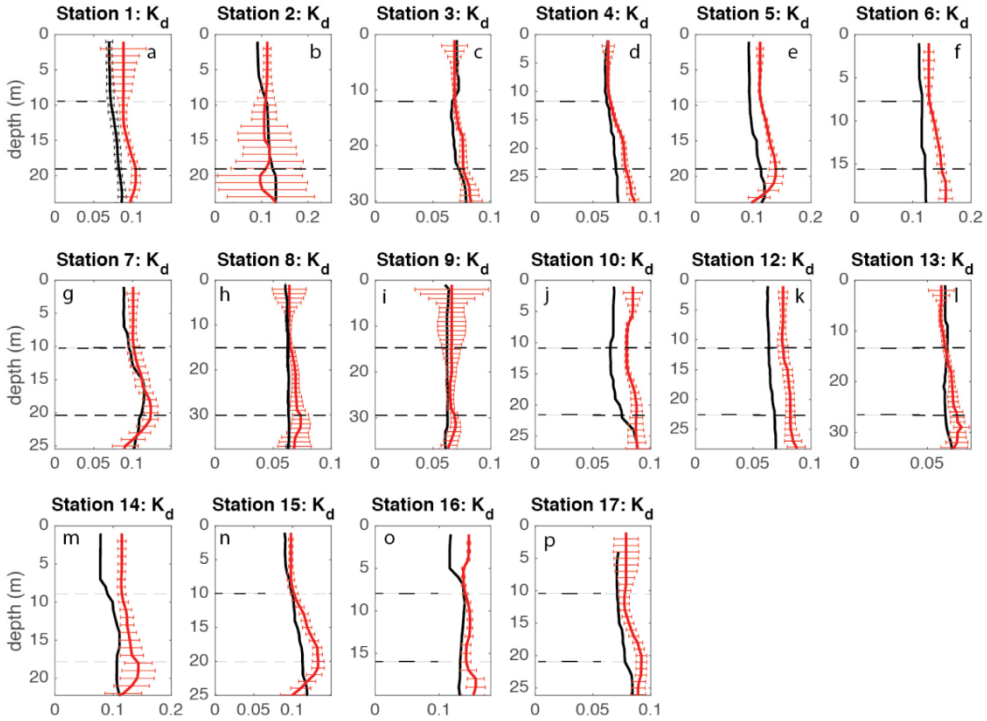

Fig. 5. HSRL-1 and *in situ* measurements of K_d (m^{-1}). The black profiles are the *in situ* measurements where panels (a) and (h) show the stations with replicate casts ($\Delta t < 1$ day, same station) with the error bars representing one standard deviation. The red profiles are the HSRL-1 measurements (median of ten nearest profiles to *in situ* cast) with the error bars representing one standard deviation within profiles. The error bars are a measure of the spatial variability around each station. The dotted lines show the first and second optical depths.

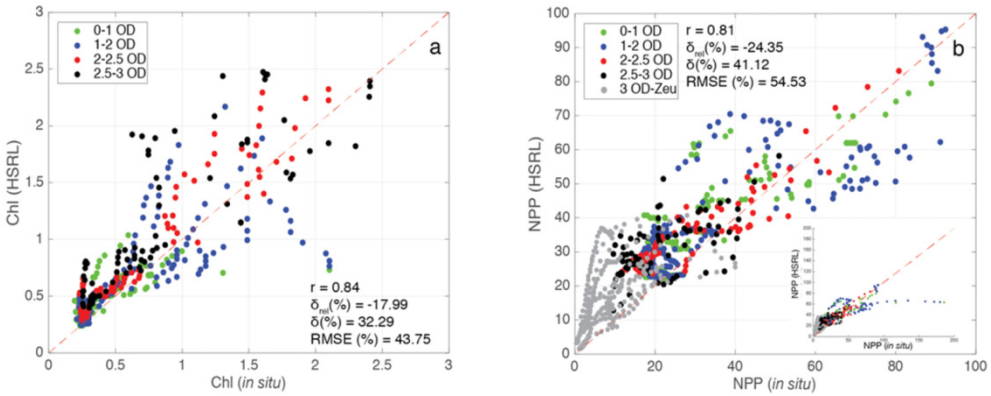

Fig. 6. HSRL-1 and *in situ* measurements of (a) chlorophyll a (Chl; mg m^{-3}) and (b) net primary production (NPP; mg m^{-3} d^{-1}). The inset in panel (b) shows the full range of data with x and y-axes limits set to 200 mg $m^{-3}d^{-1}$. The red lines show the 1:1 relationship.

The carbon-based production model (CbPM) employs information on chlorophyll concentration to characterize physiological variability within plankton communities. The HSRL-1 currently does not retrieve chlorophyll directly so we made a first order calculation of chlorophyll from HSRL-1 b_{bp} data using the chlorophyll:C_{phyto} relationship of Westberrry et al. (2008) [11]. Vertical profiles of chlorophyll calculated in this manner (Eqs. (1a) and (1b) from the HSRL-1 data exhibited a significant correlation with *in situ* optically-based

Optics EXPRESS

chlorophyll values (r = 0.84) (Fig. 6(a)). Given the temporal variability in vertical plankton properties discussed above and the implications this has on profiles of NPP, we observed an exceptional correlation between HSRL-1 and *in situ* optics-based NPP values (r = 0.81) (Fig. 6(b)). Stations 11 and 18 were not included in this analysis because there were no spatial matchups fitting distance criteria.

4. Discussion

Passive ocean observing sensors do not measure subsurface structure in ocean properties, resulting in errors in water column integrated phytoplankton biomass, light attenuation, and NPP estimates. *In situ* data show relative errors of up to 45.6% and 36.3% in phytoplankton biomass and light attenuation, respectively, when compared to no vertical structure. Measured ocean properties were underestimated at every station relative to *in situ* data and NPP errors up to 54% were observed when the vertically-weighted surface data were used. Furthermore, the vertical structure observed during SABOR does not capture the full range of variability globally, so the potential errors in products derived from ocean color are likely to be even larger than measured during this field campaign. Our findings, therefore, indicate that the ability to resolve upper ocean vertical structure in phytoplankton stocks and the underwater light field significantly improves estimates of NPP over 'ocean color type' values.

The largest proportional errors in integrated NPP were associated with biomass features above two optical depths. These results are consistent with the conclusions of Churnside (2015) [1] who found that using passive remote sensing methods introduced significant errors to NPP estimates when subsurface phytoplankton layers were present and this error was largest when the chlorophyll layer was located in the upper water column. The penetration depth expected for an ocean-optimized satellite lidar is within this upper zone which suggests that a satellite ocean-optimized lidar would significantly improve global estimates of integrated phytoplankton biomass and NPP.

Matchups between *in situ* and HSRL-1 measurements were good with correlation coefficients for b_{bp} and K_d of 0.94 and 0.90, respectively, despite the high spatial and temporal variability that characterizes the SABOR region. This is quite remarkable given that point measurements from *in situ* profiles were compared to measurements averaged up to 70 km away (see Table 1). The different spatial and temporal resolutions between measurements likely contributed to the observed discrepancies in matchups.

Although SABOR provided several coincident matchups between HSRL-1 and *in situ* optics, the data are still limited. An important avenue for future studies will be to expand matchup analyses with data from a broader range of environmental conditions, such as data collected as part of the NAAMES (North Atlantic Aerosols and Marine Ecosystems Study) campaign. Such comparative analyses between coincident HSRL-1 and *in situ* measurements will provide important information for evaluating science objectives and design criteria for a future ocean-optimized space-based lidar.

The current study demonstrates the utility of the HSRL technique for depth-resolved profiles on b_{bp} and K_d, which, by analogy to the improvements achieved with the depth-resolved *in situ* data, would enable much higher accuracy in remote-sensing estimates of NPP. Applying the technique at more than one wavelength could provide even greater accuracy in NPP. The more advanced NASA HSRL-2 instrument currently implements the HSRL technique at both 355 and 532 nm for atmospheric measurements and is in the process of being upgraded for higher vertical resolution (~1 m) to optimize it for ocean profiling. Measurements of K_d at these two wavelengths will enable separation of different ocean constituents contributing to the attenuation of light in the water column, e.g., colored dissolved organic matter (CDOM), which is the primary light-absorbing agent in the UV spectrum. The light attenuation coefficient is a function of scattering and absorption, and since the backscattering coefficient is directly measured by the HSRL, the only unknown property is absorption, which includes absorption by CDOM, water, and particles, including

Optics EXPRESS

phytoplankton. Chlorophyll (i.e., phytoplankton absorption) could thus be calculated directly by subtracting from K_d the effects of scattering and CDOM and water absorption. The effects of nutrient limitation on chlorophyll:C_{phyto} are accounted for in this calculation and thus represent an improvement over the methods used here. Chlorophyll is a critical variable for most NPP algorithms, particularly because of the information it provides on phytoplankton physiology when retrieved concurrently with independent estimates of biomass. Improvements in the estimation of vertical profiles of chlorophyll are critical for improving NPP results.

We are entering a new era in satellite oceanography where satellite lidar observations can address many of the issues that challenge passive ocean color techniques. Already, observations from the CALIOP lidar have been used to quantify global stocks of C_{phyto} and total POC and to evaluate complete annual plankton cycles in the polar regions that are particularly problematic for passive sensors [28,29]. Despite these successes, the CALIOP lidar sensor has limitations for ocean retrievals. First, CALIOP was designed for atmospheric applications and its vertical binning resolution (22.5 m) is too coarse for retrieving information on vertical structure in the oceans. Second, CALIOP is unable to directly separate the backscatter and attenuation coefficients. Behrenfeld et al. (2013) [28] retrieved b_{bp} estimates from CALIOP by using independent estimates of K_d from the MODIS passive ocean color sensor and an estimate of the reflectance of the laser beam from CloudSat radar surface reflection data or wind speed data from the Microwave Scanning Radiometer-EOS. In the subsequent polar-focused study of Behrenfeld et al. (2016) [29], an empirical relationship between lidar depolarization and K_d was used to retrieve b_{bp}, due to lack of coincident ocean color data particularly during the winter months. These parameterizations have been tested from data acquired on episodic intervals during which CALIOP was pointed 30° off nadir to minimize the laser surface reflection. However, the parameterization scheme for nominal near-nadir operations were still dependent on an empirically derived relationship between collated MODIS and CALIOP b_{bp} and K_d at lower latitudes [29]. Major advantages over the standard elastic backscatter lidar approach of CALIOP is achieved via the HSRL technique. HSRL permits independent, direct retrievals of b_{bp} and K_d with minimal assumptions and no reliance on ancillary data. This major advantage, along with the high vertical-resolution sampling (~1 m), allowed the HSRL-1 instrument to collect vertically resolved retrievals of K_d and phytoplankton biomass during SABOR. While an HSRL has not yet been flown in space, there is no technological barrier to either implementing the technique or achieving high vertical resolution (e.g., 3 m) for ocean profiling. Such an instrument flown in space would provide independent and more accurate ocean property retrievals than a standard CALIOP-like backscatter lidar and an enormous independent data set to evaluate and improve passive ocean color retrievals.

Funding

National Atmospheric and Space Administration (NASA) grants NNX15AI15G, NNX15AF30G, and NNX15AN17G.

Acknowledgments

We thank James Churnside for his numerous invaluable discussions. We thank Nicole Stockley for support with *in situ* data collection. We acknowledge Kimberley Halsey and Jason Graff for providing *in situ* chlorophyll, carbon, and NPP data for comparisons to optics-based values and for their insightful comments. We additionally thank the captain and crew of the *R/V Endeavor*.